

# Melatonin alleviates senile osteoporosis by regulating autophagy and enhancing fracture healing in aged mice

From Zhejiang University of Medicine, and Key Laboratory of Oral Biomedical Research of Zhejiang Province, Hangzhou, China

D. Zhang,<sup>1</sup> T. Zhu,<sup>1</sup> J. Bai,<sup>1</sup> C. Chen,<sup>1</sup> J. Wen,<sup>1</sup> Y. Zhou,<sup>1</sup> X. Guan<sup>1</sup>

The Affiliated Hospital of Stomatology, School of Stomatology, Zhejiang University of Medicine, and Key Laboratory of Oral Biomedical Research of Zhejiang Province, Hangzhou, China

Cite this article:

*Bone Joint Res* 2025;14(2): 97–110.

DOI: 10.1302/2046-3758.142.BJR-2024-0112.R2

Correspondence should be sent to Xiaoxu Guan  
7312020@zju.edu.cn

## Aims

In our previous research, we have found that melatonin (MEL) affects the osteoporotic process. By balancing bone remoulding, autophagy is involved in age-related bone loss. However, as a regulator of autophagy, whether MEL influences senile osteoporosis via regulating autophagy remains unclear.

## Methods

Cellular, radiological, and histopathological evaluations were performed on 36 16-month-old male C57BL6/L mice or aged bone marrow-derived mesenchymal stem cells. A MEL-gelatin methacrylamide system was constructed to aid osteoporotic fracture healing.

## Results

In this study, we found that bone loss, low level of MEL, and decreased autophagy coexisted in aged C57BL6/L mice. A physiological (low, 10 nM but not 100 nM) concentration of MEL restored bone loss, transformed the cytokine framework, and increased the autophagic level in aged mice, whereas inhibition of autophagy unfavourably reduced the positive effects of MEL on bone mass. The autophagy-conducted increased osteogenic lineage commitment and extracellular matrix mineralization, but not matrix synthesis of aged bone marrow-derived mesenchymal stem cells, was responsible for MEL anabolic effects on bone. *PIK3C-AKT-MTOR* signal was tested to be a main pathway that is involved in MEL-induced autophagy.

## Conclusion

Our data suggest that the application of MEL can restore degenerative osteogenesis of aged bone marrow-derived mesenchymal stem cells, and has the potential to regain bone mass in aged mice through activating autophagy via the *PIK3C-AKT-MTOR* pathway. MEL therefore may serve as a potential clinical therapy to treat senile osteoporosis.

## Article focus

- This study focuses on the mechanism of melatonin (MEL)-induced autophagy in rescuing senile osteoporosis and potential to enhance fracture healing.

## Key messages

- MEL at a physiological concentration reverses bone loss and boosts autophagy in aged mice, positively impacting bone health.
- Autophagy plays a pivotal role in MEL-induced osteogenesis by promoting osteogenic lineage commitment and

extracellular matrix mineralization in aged bone marrow-derived mesenchymal stem cells (BMMSCs).

- The *PIK3C-AKT-MTOR* signalling pathway is implicated in MEL-induced autophagy, and the development of a MEL-methacrylated gelatin (GelMA) system holds promise for enhancing bone fracture healing in senile osteoporosis models.

## Strengths and limitations

- The role of MEL-induced autophagy in rescuing senile osteoporosis was revealed for the first time.

- We established a MEL-GelMA system applied to the bone fracture model in aged mice.
- The study lacked experimental evidence for human cells.

## Introduction

Osteoporosis is a prevalent metabolic bone disorder characterized by an increased risk of fractures due to diminished bone density and quality. It is primarily categorized into three distinct forms: postmenopausal osteoporosis, juvenile osteoporosis, and senile osteoporosis.<sup>1</sup> With the extension of human lifespan and the formation of an ageing society, the prevalence of senile osteoporosis in the elderly population is substantially higher.<sup>2</sup> Senile osteoporosis leads to a significantly increased incidence of bone fractures due to reduced bone mass and heightened bone fragility, profoundly impacting the quality of life in the elderly population. Consequently, senile osteoporosis has garnered considerable attention in both clinical and research settings.

Decreased bone mass observed in senile osteoporosis is generally associated with changes in the bone microenvironment, including alterations in cytokine levels and the function of bone marrow-derived mesenchymal stem cells (BMMSCs). With ageing, BMMSCs exhibit reduced osteogenic differentiation, which may be attributed to the diminished autophagy.<sup>3</sup> Regaining the ability of cell autophagy could be an effective approach to recover the osteogenic ability of BMMSCs and regain bone mass lost in senile osteoporosis.

Autophagy is a catabolic process balancing cellular homeostasis, in which eukaryotic cells degrade cell components such as damaged mitochondria and proteins by autophagosomes and lysosomes.<sup>4</sup> Autophagy can enhance free radical scavenging and protect cells in many physiological and pathological conditions such as cancer, ageing, neurodegeneration,<sup>4</sup> and osteoporosis.<sup>5</sup> Recent literature has elucidated the relationship between autophagy and oxidative stress, highlighting their involvement in various pathological conditions.<sup>4</sup> The roles of antioxidants in the prevention against pathological processes, such as senile osteoporosis, should be extensively researched.

Melatonin (MEL) is an indoleamine neuroendocrine hormone synthesized and secreted mainly by the pineal gland. It has multifold biological functions, such as regulating biological rhythms, immune regulation, and anti-tumour effects.<sup>6</sup> MEL has been shown to improve postmenopausal osteoporosis via the *BMAL1/ROS/MAPK-p38* pathway.<sup>7</sup> As an autophagy regulator, MEL also plays a beneficial role against various diseases.<sup>4</sup> In line with these findings, secretion of MEL is tensely related to bone physiology and can promote anabolic effects on bone.<sup>8</sup> It has also been confirmed that MEL levels decline with ageing in both serum and the pineal gland,<sup>9</sup> which may contribute to bone loss and reduced autophagy observed in age-related osteoporosis. However, its role as a regulator of autophagy in the context of senile osteoporosis has not been thoroughly investigated.

## Methods

### Reagents and antibodies

MEL, ascorbic acid, and  $\beta$ -glycerol phosphate were purchased from Sigma-Aldrich (USA). The autophagy inhibitor 3-MA and PI3K activator 740-YP were purchased from MedChemExpress

(Sweden). Primary antibodies included rabbit monoclonal anti-Runx2 (Cat# 12556S; Cell Signaling Technology (CST), USA), rabbit monoclonal anti-Osterix (Cat# ab209484; Abcam, UK), rabbit monoclonal anti-osteocalcin (OCN) (Cat# ab93876; Abcam), rabbit polyclonal anti-collagen I (Col-I) (Cat# 14695-1-AP; Proteintech, USA), rabbit monoclonal anti-LC3B (Cat# 2775; CST, USA), rabbit monoclonal anti-BECLIN1 (Cat#3738; CST), rabbit polyclonal anti-ATG7 (Cat#2631; CST), rabbit polyclonal anti-anti-PIK3R1/p85 (Cat#4292S; CST), rabbit monoclonal anti-p-PIK3R1/p85 (Cat#4228S; CST), rabbit monoclonal anti-AKT (Cat#4691; CST), rabbit monoclonal anti-p-AKT (Cat#4060; CST), rabbit monoclonal anti-MTOR (Cat#2972S; CST), rabbit monoclonal anti-p-MTOR (Cat#2971S; CST), rabbit monoclonal anti-TSC2 (Cat#4308; CST), rabbit monoclonal anti-p-TSC2 (Cat#3617; CST), and rabbit monoclonal antiglyceraldehyde-3-phosphate dehydrogenase GAPDH (BK7021; Baoket Technology, China).

### Animals

All animal procedures were approved by the Institutional Animal Care and Use Committee of Zhejiang University (No. ZJU20220168), and all operations on animals followed the guidelines of the Guide for the Care and Use of Laboratory Animals-Eighth Edition.<sup>10</sup>

Young (two-month-old) C57BL/6J male mice and aged (16-month-old) C57BL/6J male mice were housed under controlled light conditions (12 hours day/night cycle) in specific pathogen-free conditions with free access to food pellets and tap water. Aged mice were randomly divided into three groups ( $n = 6$  in each group). The control group was treated with vehicle reagents, and the MEL and MEL + 3MA groups were treated with MEL (50 mg.kg<sup>-1</sup> body weight per day) or MEL (50 mg.kg<sup>-1</sup> body weight per day) + 3MA (15 mg.kg<sup>-1</sup> body weight per day) oral gavage for two months. Drug administration was carried out blindly. Blood was gathered from the lateral canthus vein before mice were killed by cervical dislocation, and the fresh tibia and femur were fixed with 4% paraformaldehyde or frozen with liquid nitrogen. An ARRIVE checklist is included in the Supplementary Material to show that the ARRIVE guidelines were adhered to in this study.

### Bone $\mu$ CT analysis

Excised mice femora were analyzed by the MILabs U-CT-OI imaging system (MILabs, Netherlands), using a 80 KV voltage, 240 $\mu$ A current. The region of interest (ROI) was the 1 mm thick area 0.5 mm proximal away from the growth plate. The bone mineral density (BMD), trabecular bone volume per total volume (BV/TV), trabecular bone thickness (Tb.Th), trabecular bone separation (Tb.Sp), and trabecular bone number (Tb.N) were assessed with BoneJ (University of Southern Denmark, Denmark) as previously described.<sup>11</sup> The images of bone structure were reconstructed by this software.

### BMMSC isolation, culture, and transfection

BMMSCs were isolated from young (two-month-old) or aged (16-month-old) C57BL/6J mice as previously described.<sup>12</sup> In short, the BMMSCs were obtained by repeatedly flushing the dissected tibia and fibula by a syringe. Then, BMMSCs were plated in 10 cm culture dishes with  $\alpha$ -minimum essential medium (Basalmedia Technologies, China) containing 15%

foetal bovine serum (FBS; Bovogen Biologicals, Australia), 100  $\mu\text{g ml}^{-1}$  streptomycin, and 100 U  $\text{ml}^{-1}$  penicillin at 37°C with 5%  $\text{CO}_2$ . The culture medium was changed every two to three days, and 0.25% trypsin was employed to digest the cells once they were 70% to 90% confluent. Suspension cells were then passaged in ordinary culture medium consistent with the above, and then osteogenic differentiation medium ( $\alpha$ -MEM with 15% FBS,  $10^{-2}$  M  $\beta$ -glycerol phosphate and 50 mg/ml ascorbic acid) was applied to induce the differentiation. BMMSCs from passage one were used for our experiments. BMMSC cells from aged mice were transfected stably with full-length Rheb<sup>D64L</sup> cDNA or Rheb<sup>D60K</sup> cDNA, which were established or packaged by Mailgene Biotechnology (China).

#### Senescence-associated $\beta$ -galactosidase staining

The BMMSCs ( $1 \times 10^5$  cells per well) were planted onto the bottom of a 12-well plate and cultured for three days.  $\beta$ -gal staining kit (Beyotime Institute of Biotechnology, China) was used to assess  $\beta$ -gal activity following the provided protocol. The numbers of senescent cells that were stained blue were counted, and the percentage was calculated. Blue-stained cells (senescent cells) from five regions were randomly selected and counted under a microscope (magnification,  $\times 100$ ) (Olympus, Japan). Then, the percentage of total cells was calculated.

#### Cell proliferation assays

Cell Counting Kit-8 (CCK-8; Beyotime Institute of Biotechnology) was employed to analyze cell proliferation. BMMSCs ( $1 \times 10^4$  cells per well) were planted onto the bottom of 96-well plates exposed to MEL of different doses for three, five, or seven days. After treatment, CCK-8 solution was added according to the provided protocol into each well after removal of the supernatants. The absorbance was assessed at 450 nm with a Multiskan Spectrum Microplate Spectrophotometer (Thermo Fisher Scientific, USA).

#### Quantitative real-time RT-PCR

Quantitative real-time reverse transcriptase polymerase chain reaction (RT-PCR) assay was used to measure the gene expression levels of cells or extracted bone marrow tissues. The total messenger RNA (mRNA) was extracted from BMMSCs with the RNAiso Plus (TaKaRa Biotechnology; Japan). Reverse transcription was then performed with the PrimeScript RT Reagent Kit (TaKaRa Biotechnology). ViiATM7 Real-Time PCR System (Applied Biosystems, USA) was applied to perform quantitative RT-PCR assays with SYBR Premix Ex Taq<sup>TM</sup> Kit (TaKaRa Biotechnology) following the provided instructions. The detailed sequences of the primers for each gene are listed in Supplementary Table i. The gene *gapdh* was applied as the internal reference. The  $\Delta\Delta CT$  method was applied to measure the relative gene expression levels.

#### Western blot

Cells or extracted bone marrow tissues were harvested and lysed with radioimmunoprecipitation assay (RIPA) lysis buffer and kept for 30 minutes at 4°C. The total protein concentration of supernatants from centrifugal for 15 minutes at 12,000 rpm at 4°C was assessed with bicinchoninic acid (BCA) protein assay reagent (Beyotime). Next, 20 to 40  $\mu\text{g}$  per sample were separated and loaded on sodium dodecyl sulfate polyacrylamide gel electrophoresis (SDS-PAGE) gels

and transferred onto polyvinylidene fluoride (PVDF) membrane (Merck Millipore, Germany). Then, 5% skim milk was used to block the membrane for one to two hours and afterwards incubated in primary antibodies overnight at 4°C against runt-related transcription factor 2 (Runx2) (1:1,000), sp7 transcription factor (Osterix) (1:1,000), osteocalcin (OCN) (1:1,000), type I collagen (Col-I) (1:1,000), microtubule-associated protein 1A/1B-light chain 3 beta (LC3B) (1:1,000), BECLIN1 (1:1,000), autophagy related protein 7 (ATG7) (1:1,000), sequestosome 1 (P62) (1:1,000), phosphoinositide 3-kinase (PI3K) (p-100) (1:1,000), phosphorylated phosphoinositide 3-kinase (p-PI3K) (1:1,000), RAC-alpha serine/threonine-protein kinase (AKT) (1:1,000), phosphorylated AKT (p-AKT) (1:1,000), mechanistic target of rapamycin (MTOR) (1:1,000), phosphorylated MTOR (p-MTOR) (1:1,000), tuberous sclerosis complex 2 (TSC2) (1:1,000), phosphorylated TSC2 (p-TSC2) (1:1,000), and glyceraldehyde-3-phosphate dehydrogenase (GAPDH) (1:10,000). After being washed in tris-buffered saline with tween 20 (TBST) three times for ten minutes, membranes were incubated in anti-rabbit horseradish peroxidase (HRP)-conjugated secondary antibody (1:10,000) for two hours at room temperature. After being washed by TBST three times for ten minutes again, the protein bands were treated with ECL kit (Beyotime) and then visualized with the ChemDoc MP Imaging System (Bio-Rad, USA) following provided protocol. Image Lab 5.2.1 software (Bio-Rad) was used to quantify the results. GAPDH was regarded as an internal reference.

#### Alkaline phosphatase analysis

Alkaline phosphatase (ALP) staining and ALP activity assays were conducted using a BCIP/NBT Alkaline Phosphatase Color Development Kit and an Alkaline Phosphatase Assay Kit (both from Beyotime), following the manufacturer's protocol. After BMMSCs were cultured in osteogenic differentiation medium for seven days, ALP staining was performed following fixation with 4% paraformaldehyde for 15 minutes. ALP activity was measured at 405 nm using a spectrophotometer.

#### Mineralization assay

BMMSCs were planted in osteogenic differentiation medium for 21 days, and then fixed using 4% paraformaldehyde for 15 minutes before being stained with Alizarin Red S (Beyotime) for 20 minutes at room temperature. For quantification of mineralization, 10% cetylpyridinium chloride was used to elute stain for 15 minutes, and then we analyzed the spectrophotometric absorbance at 540 nm.

#### Bone histology and immunohistochemistry

Haematoxylin and eosin (H&E) staining was used to assess the structure of bone trabeculae, while immunohistochemistry (IHC) staining was employed to visualize and analyze the expression of OCN and Osterix in bone tissue. The tibiae after decalcification were embedded using paraffin and sliced in sagittal plane for H&E and IHC staining. The regions of interest were photographed with a microscope. For IHC staining, antigen retrieval was followed by submersing slides in ethylenediaminetetraacetic acid (EDTA) buffer solution after deparaffinizing the paraffin sections. The sections were then incubated in 3% hydrogen peroxide for ten minutes and blocked with 5% bovine serum albumin for one hour at room temperature. After that, the primary antibody against

OCN (1:200) or Osterix (1:500) was added to the sections at 4°C overnight. Thereafter, the anti-rabbit HRP-conjugated antibody was applied to incubate the sections for 30 minutes at room temperature. Sections were then stained with the EnVision Detection Systems Peroxidase/DAB kit (Dako, Denmark) and counterstained with haematoxylin. Tartrate-resistant acid phosphatase (TRAP) staining was performed to detect osteoclasts, following the protocol provided with the TRAP staining kit from Sigma-Aldrich. Finally, sections were mounted with coverslips and observed under a microscope. Six random fields on each H&E- or TRAP-stained section were photographed at  $\times 400$ , and the osteoblast/osteoclast number and bone perimeter/area on each microscopic image were determined. The mean number of osteoblasts per bone perimeter (Ob.N/B.Pm) and number of osteoclasts per tissue area (Oc.N/T.Ar,  $\text{mm}^{-2}$ ) were reported according to the guidelines by the American Society for Bone and Mineral Research Nomenclature Committee.<sup>13</sup> Histomorphometric analysis was carried out using OsteoMetrics software (Osteometrics, USA) to determine the area of new bone and new fibrous and cartilage tissue, as presented in Supplementary Figure a.<sup>14</sup>

Image-Pro Plus software (Media Cybernetics, USA) was applied to calculate the IHC integral optical density (IOD), Ob.N/B.Pm, and Oc.N/T.Ar,  $\text{mm}^{-2}$ . The IHC assay was performed according to the *British Journal of Pharmacology* guidelines.<sup>15</sup>

#### Enzyme-linked immunosorbent assay

The concentration of tartrate-resistant acid phosphatase 5 (ACP5), OCN, MEL, in mouse serum were measured with Mouse Tartrate Resistant ACP5 ELISA Kit, Mouse Osteocalcin ELISA Kit, and Mouse Melatonin ELISA Kit (Elabscience Biotechnology, China), respectively, according to the manufacturer's instructions.

#### Bone fracture model

Aged (16-month-old) C57BL/6J male mice were used to establish a bone fracture model. All surgical procedures were conducted under isoflurane anaesthesia. Following hair removal with clippers and depilatory cream, the surgical sites were sterilized with 2% iodophor. After the surgery, the visceral lining or muscle was sutured, and the skin was closed with absorbable sutures, which were removed two weeks postoperatively. Oral Meloxicam (2.0 mg/kg) and intraperitoneal Buprenex (0.5 mg/kg) were administered as anti-inflammatory analgesics preoperatively, and once every 24 hours postoperatively for three days.

Bone fracture in aged mice was performed as previously described with some modifications.<sup>16</sup> In brief, a small incision above the right anterolateral femur was performed to expose the patella and femur following surgical site sterilization and anaesthesia. Then, a 27-gauge syringe needle was applied to insert along the long axis of the femur from the patellar groove to the bone marrow cavity. After removing the needle, fracture was performed at the middle of the femoral diaphysis using a diamond thin cutting wheel on a dremel saw (Cat#100230-724; VWR, USA). To fix the fracture, another needle of 25-gauge was inserted into the bone marrow cavity through the hole made at the patellar groove, and then trimmed to protect the patella-femoral joint space. Before closing the skin with wound clips, muscle was then put back

to the fracture site and closed using 5-0 absorbable sutures. Alternatively, same volume (0.8 ml) of GelMA, GelMA-MEL, and GelMA-MEL-3MA was wrapped around the surgical fracture and photocured immediately. All animals were euthanized by CO<sub>2</sub> four weeks postoperatively. The compressive modulus, percentage mass remaining after four weeks, and mass swelling ratio of the three material systems were tested according to our previous research to evaluate their mechanical stability, degradation behaviour, and swelling characteristics.<sup>17</sup>

#### Bioinformatic analysis

Total RNA sequencing (RNAseq) data were extracted from the BMMSCs from tibia and fibula according to the instruction manual of the TRIzol Reagent (Life Technologies, Thermo Fisher Scientific). RNA integrity and concentration were checked using an Agilent 2100 Bioanalyzer (Agilent Technologies, USA). The mRNA was isolated by NEBNext Poly (A) mRNA Magnetic Isolation Module (E7490; New England Biolabs (NEB), USA). The complementary DNA (cDNA) library was constructed following the manufacturer's instructions of NEBNext Ultra RNA Library Prep Kit for Illumina (E7530; NEB) and NEBNext Multiplex Oligos for Illumina (E7500; NEB). In brief, the enriched mRNA was fragmented into approximately 200nt RNA inserts, which were used to synthesize the first-strand cDNA and the second cDNA. The double-stranded cDNA was performed end-repair/dA-tail and adaptor ligation. The suitable fragments were isolated by Agencourt AMPure XP beads (Beckman Coulter, USA), and enriched by PCR amplification. Finally, the constructed cDNA libraries were sequenced on a flow cell using an Illumina HiSeq sequencing platform. Gene expression levels were estimated using FPKM (fragments per kilobase of exon per million fragments mapped) values by the Cufflinks software (The Trapnell Lab, University of Washington, USA).

Genes related to senile osteoporosis were predicted using the Genecard database,<sup>18</sup> DisGeNET database,<sup>19</sup> and OMIM database.<sup>20</sup> The expression levels were compared using heatmap in R software version 3.6.1 (R Foundation for Statistical Computing, Austria) based on the mean values after removing discrete values with low credibility. DAVID server (National Institute of Allergy and Infectious Diseases, USA) was applied to analyze the gene function and pathway enrichment. Potential candidate targets were input to DAVID server using Kyoto Encyclopedia of Genes and Genomes (KEGG) databases or WikiPathways database.

#### Data and statistical analysis

Experimental data are presented as the mean and SD. Comparisons were assessed by an independent-samples *t*-test, one-way analysis of variance (ANOVA), or Fisher's exact test. Tukey's post-hoc test was applied when the *F* value in ANOVA turned out to be statistically significant ( $p < 0.05$ ), and there was no significant variance inhomogeneity. GraphPad Prism 8 statistical software (GraphPad Software, USA) was applied for the statistical analysis. All experiments were repeated at least three times.  $p < 0.05$  was considered to be statistically significant.

In vivo and in vitro researches and group experiments followed the principle of randomization, equalization, and blinding, through the process of experimental performance,

mouse allocation, and data extraction and analysis. Six mice were assigned to each group in vivo animal experiments to ensure the implementation of statistical analysis. As for the in vitro study, the group size was at least five to obtain the suitable group size for statistical analysis. All group sizes represent the numbers of experimental independent biological repeats, and statistical analysis was performed using these independent values.

Results were statistically analyzed only in groups whose size was more than five, and every data point was included for the statistical analysis in every test. Data normalization was performed to decrease variation. 'Fold change' was defined as values that were divided by the mean of control values in results of quantitative evaluation of Alizarin Red S staining, ALP activity, oil red staining, enzyme-linked immunosorbent assay (ELISA), and quantitative real-time RT-PCR. Also, the y-axis in the figures was labelled with 'fold mean of the controls'. In particular, for results of the ALP activity, we used 'p-nitrophenol amount per total protein amount per minute' formula to normalize data to fold mean of the control data. For results of ELISA, we normalized detected protein concentrations that were divided by the total protein to fold mean of the controls. For the quantitative real-time RT-PCR results, we used the  $\Delta\Delta CT$  method to calculate the relative gene expression. The data were normalized by comparing them to the fold mean expression of the control group, ensuring that variations in gene expression were due to the experimental treatment rather than technical errors.

## Results

### MEL restored degenerative osteogenesis at suitable concentration (10 to 100 nM) in aged BMMSCs

To validate the fidelity of the senile osteoporosis animal model, femora from young (two-month-old) and aged (16-month-old) mice were harvested for bone structure analysis. Micro-CT (Figure 1a) and H&E staining (Figure 1b) were performed to examine the femora. In aged mice, BMD, trabecular bone volume/total volume (BV/TV), trabecular thickness (Tb.Th), and trabecular number (Tb.N) were decreased, while trabecular spacing (Tb.Sp) was increased compared to young mice (Figure 1c).

BMMSCs from young (two-month-old) and aged (16-month-old) femora were harvested and cultured to analyze cell biological properties. Senescence-associated  $\beta$ -galactosidase analysis (SA- $\beta$ -gal) showed that more  $\beta$ -gal-positive cells existed among aged BMMSCs (Supplementary Figures ba and bb). The osteogenesis capacity of BMMSCs from aged mice was reduced compared with those harvested from young mice, which was evident in ALP staining and Alizarin Red staining (Figures 1d and 1e). In line with the staining results, the levels of the osteogenic genes *runx2*, *col-1*, *osterix*, and *ocn* were significantly decreased in BMMSCs from aged mice (Supplementary Figure bc).

Enrichment analysis of genes related to senile osteoporosis predicted using the Genecard database, DisGeNET database, and OMIM database using WikiPathways revealed significant enrichment of genes related to senile osteoporosis within MEL metabolism and its effects, suggesting a potential influence on the development of senile osteoporosis (Figure 1f). Serum MEL level analyzed by ELISA

showed that the concentration in serum was notably lower in aged mice than in young mice (Figure 1g).

To determine the suitable concentration of MEL to promote the osteogenic differentiation in vitro, we performed ALP staining (Figure 1h), ALP activity test (Figure 1i), Alizarin Red S staining (Figure 1j), and quantification of Alizarin Red staining (Figure 1k) to evaluate the treatment effects. MEL of optimal concentration (10 nM and 100 nM) increased osteogenesis significantly in aged BMMSCs (Figures 1h to 1k), while excessive or minimum concentration (1 nM, 1  $\mu$ M, 10  $\mu$ M) exerted no effects on ALP level or even played a negative role (Supplementary Figures ca and cb). The negative influence of excessive dose of MEL on cell proliferation might partly be the reason that these outcomes were reached (Supplementary Figures cc and cd). After treatment for five to seven days, 10 nM and 100 nM MEL did not influence cell proliferation in aged BMMSCs (Supplementary Figures ce and cf). Although there was no evident difference in the deposited calcium after 10 nM and 100 nM MEL treatment, aged BMMSCs exposed to 10 nM MEL showed higher ALP activity level (Figure 1i).

The gene expression levels of early osteogenic markers *runx2* and *osterix* were increased only in aged BMMSCs treated by 10 nM MEL (Supplementary Figure ce). However, the expression of bone matrix marker *col-1* was unaffected by MEL treatment in both young and aged mice (Supplementary Figure ce). Consistent with the early osteogenic markers, the expression level of *ocn*, primarily expressed in mature osteoblasts, was also elevated in aged BMMSCs treated with 10 nM MEL, but not with 100 nM (Supplementary Figure cf). In line with these findings, the *opg/rankl* ratio reflecting osteoclast function during bone remodelling was increased in aged BMMSCs treated by MEL of 10 nM (Supplementary Figure cg). Consequently, an optimal concentration of 10 nM was applied in subsequent assays. All primer sequences used in RT-PCR are provided in Supplementary Table i.

These data indicate that bone structure deteriorates with ageing in the animal model, and osteogenesis shows a declining trend in aged BMMSCs. The onset of senile osteoporosis is associated with a reduction in MEL levels. The application of MEL may restore degenerative osteogenesis, with a suitable concentration (10 nM) enhancing osteogenesis and influencing osteoclast function in aged BMMSCs.

### MEL increased autophagic level and restored degenerative osteogenesis by upregulating the autophagy level in aged BMMSCs

The analysis (GSEA) of RNA sequencing data from aged BMMSCs treated with MEL suggests that MEL strongly influences the downregulation of negative regulation of autophagy (Figure 2a). This means that MEL might be enhancing autophagy by reducing its inhibition, and this process is likely one of the primary mechanisms through which MEL promotes osteogenesis. In short, MEL-induced osteogenesis is associated with modulating the autophagy process in these stem cells (Figure 2a). Heatmaps of gene expression included in the aforementioned biological process are shown in Figure 2b. We then investigated a possible role for autophagy in MEL-induced osteogenic capacity. Western blot showed that LC3BII/I, Beclin-1, and ATG7 were increased at protein level treated with MEL of 10 nM (Figure 2c).

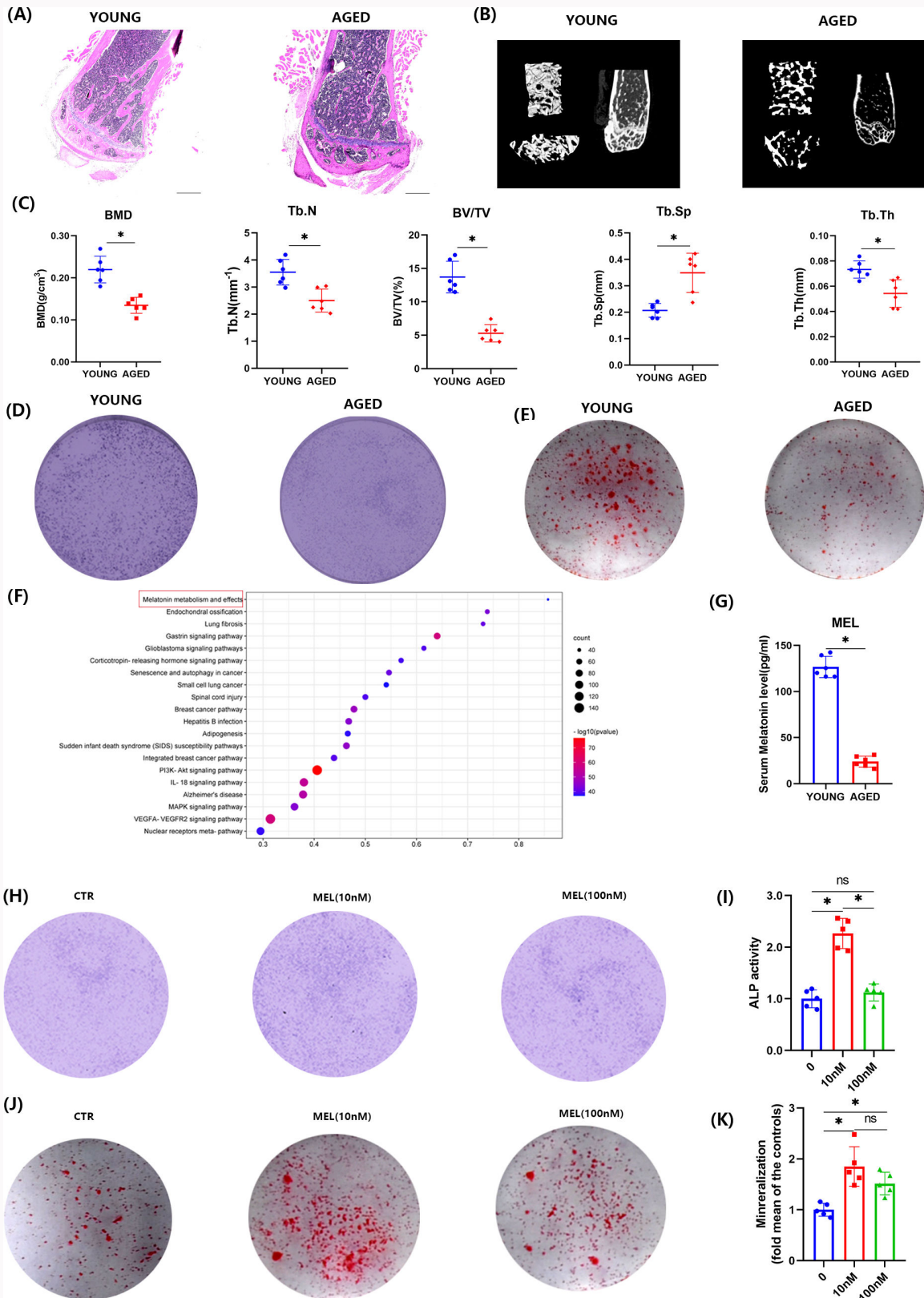


**Fig. 1**

Aged bone marrow-derived mesenchymal stem cells (BMMSCs) showed degenerative properties in osteogenesis and melatonin (MEL) promoted osteogenesis of aged BMMSCs. a) Haematoxylin and eosin (H&E) staining (40 $\times$ ) of proximal tibiae and b) micro-CT ( $\mu$ CT) imaging of distal femora of aged and young mice. c) Bone microstructure parameters such as bone mineral density (BMD), trabecular bone volume per total volume (BV/TV), trabecular bone thickness (Tb.Th), trabecular bone number (Tb.N), and trabecular bone separation (Tb.Sp). An independent-samples t-test was used to calculate the p-value in Figure 1c. d) Alkaline phosphatase (ALP) staining (20 $\times$ ) and e) Alizarin Red staining (20 $\times$ ) to analyze the osteogenesis of young and aged BMMSCs. f) Gene enrichment analysis of genes related to senile osteoporosis predicted using the GeneCards database, DisGeNET database, and OMIM database, highlighting pathways where MEL metabolism and effects showed the highest enrichment in WikiPathways. Chi-squared test was used to calculate the p-value. g) MEL in serum was analyzed by enzyme-linked immunosorbent assay (ELISA). h) ALP staining (5 $\times$ ), i) ALP level analysis, j) Alizarin Red staining (5 $\times$ ), and k) mineralization level analysis were performed. \* $p < 0.05$ , significant differences between each indicated group analyzed using one-way analysis of variance (ANOVA). CTR, control group; IL-18, interleukin-18; MAPK, mitogen-activated protein kinase; ns, not significant; PI3K-AKT, phosphoinositide 3-kinase-protein kinase B; VEGFA-VEGFR2, vascular endothelial growth factor-vascular endothelial growth factor receptor 2.

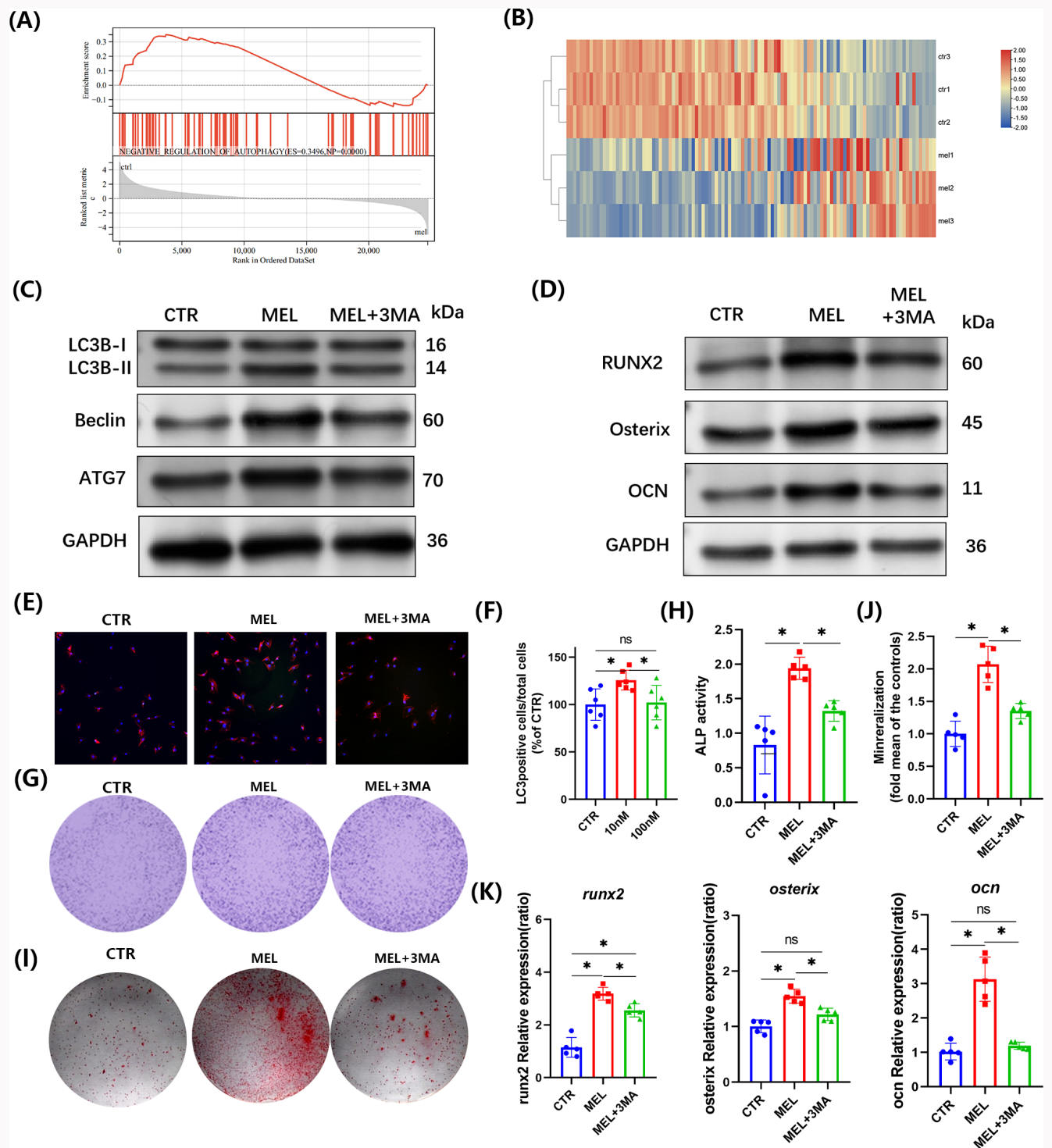


**Fig. 2**

Melatonin (MEL) induced osteogenic promotion by regulating autophagy in aged bone marrow-derived mesenchymal stem cells (BMMSCs). a) Gene set enrichment analysis (GSEA) results of negative regulation of autophagy pathway. b) Heatmaps of gene expression included in the aforementioned biological process. One-way analysis of variance (ANOVA) was used to calculate the p-value. c) Protein presentations of autophagic markers LC3B, Beclin1, and ATG7 in aged BMMSCs treated with MEL of different concentrations. d) Protein presentations of osteogenesis markers RUNX2, Osterix, and osteocalcin (OCN). e) and f) Immunofluorescence staining of LC3B (400x) and quantitative analysis of positive cells in aged BMMSCs. g) and h) Alkaline phosphatase (ALP) levels (20x) after osteogenic induction for seven days. i) and j) Mineralization levels (20x) were detected by Alizarin Red staining after 21 days of osteogenic induction. One-way ANOVA was used to calculate the p-value. k) Gene levels of osteogenesis markers *osterix*, *runx2*, and *ocn* in aged BMMSCs. Data are expressed as the mean and SD, n = 5 in each group. \*p < 0.05, significant differences between each indicated group analyzed using one-way ANOVA or an independent-samples *t*-test. CTR, control group; ES, enrichment score; GAPDH, glyceraldehyde-3-phosphate dehydrogenase; NP, normalized p-value; ns, not significant.

To further elucidate the mechanism by which MEL promotes osteogenesis in BMMSCs in vitro, we explored the relationship between autophagy and osteogenesis in aged

BMMSCs. Aged BMMSCs were treated with PBS, MEL (10 nM), or a combination of MEL (10 nM) and 3-Methyladenine (3MA) (5 mM), an autophagy inhibitor. Levels of osteogenesis-related

protein RUNX2, Osterix, and OCN improved with the treatment of MEL, while the promoting effects were counteracted with the exposure of 3MA (Figure 2d).

Accordingly, aged BMMSCs treated with 10 nM MEL accumulated more LC3B dots in immunofluorescence assay (Figures 2e and 2f). Given that 10 nM MEL demonstrated superior effects in regulating autophagy and enhancing osteogenesis in aged BMMSCs in previous experiments, this concentration was selected as the optimal dose for subsequent assays.

ALP assays, ALP activity test, Alizarin Red S staining, and quantification of Alizarin Red staining (Figures 2g to 2j) revealed that MEL could increase the osteogenic differentiation capacity of aged BMMSCs, while 3MA neutralized the promoting effects of MEL as an autophagy inhibitor. Consistent with protein expression, gene levels of *runx2*, *osterix*, and *ocn* exhibited the same trend (Figure 2k).

Our study suggests that MEL of suitable concentration (10 nM) could elevate autophagy in aged BMMSCs. Moreover, these data show that MEL could restore degenerative osteogenic capacity in aged BMMSCs, and inhibition of autophagy could reduce the positive effects of MEL on osteogenic capacity, indicating that MEL could alleviate degenerative changes in aged BMMSCs through autophagy regulation.

### MEL rescued the degenerative bone microstructure and transformed the cytokine framework via promoting autophagy level in senile osteoporosis mice

To determine whether MEL can rescue the degenerative bone microstructure and transform the cytokine framework and whether autophagy plays a key role in vivo, we used saline, MEL (50 mg.kg<sup>-1</sup> body weight per day), or MEL (50 mg.kg<sup>-1</sup> body weight per day) + 3MA (15 mg.kg<sup>-1</sup> body weight per day) to treat aged mice (16 months old). Micro-CT (Figure 3a) and H&E staining (Figure 3b) were carried out. Compared to the saline-treated group of aged mice, MEL increased bone mass effectively in aged mice (Figures 3a and 3b). Treatment with MEL led to increased BMD, in line with higher BV/TV, Tb.Th, and Tb.N, and reduced Tb.Sp (Figure 3c). Additionally, an upward trend in trabecular thickness (Tb.Th) was observed (Figure 3c), although this increase did not reach statistical significance (one-way ANOVA,  $p > 0.05$ ). Compared to the MEL-treated group, 3MA counteracted the bone-forming effect of MEL in aged mice. BMD, BV/TV, Tb.Th, and Tb.N were decreased while Tb.Sp (Figure 3c) was elevated in MEL + 3MA treated aged mice.

To investigate the underlying mechanisms of MEL's positive effects on bone mass, IHC analysis was performed. The results demonstrated that significantly higher levels of OCN and Osterix were expressed in the bone marrow of the MEL-treated group compared to the control and MEL + 3MA groups in aged mice (Figures 3d to 3f). To quantify and compare the osteoclast marker ACP5 level and the osteogenic marker OCN level in serum, commercially available ELISA kits were used according to the manufacturer's recommendation. Oral MEL supplementation decreased the ACP5 level and increased the OCN level in serum, while application of 3MA counteracted the positive effect in aged mice (Figures 3g and 3h). Oral MEL supplementation increased the serum MEL

concentration, while 3MA had no significant effect on serum MEL concentration (Figure 3i).

Taken together, these data indicate that MEL can restore bone loss, modulate the cytokine framework, and enhance autophagic activity in aged mice. The inhibition of autophagy reduces the positive effects of MEL on bone tissue, suggesting that MEL may alleviate degenerative bone structure in aged mice by promoting autophagy.

### MEL regulates autophagy via PI3K/AKT/MTOR pathways in aged BMMSCs

To explore the underlying mechanism of MEL-induced autophagy in aged BMMSCs, KEGG enrichment analysis of RNAseq from aged BMMSCs treated with or without MEL was performed for the intersection of MEL target with autophagy-related genes (Figure 4). KEGG showed *MTOR* signalling pathway and *PI3K/AKT* signalling pathway showed high enrichment. As *MTOR* pathway is one of the most important downstream signals of the *PI3K/AKT* pathway, we assumed that *PI3K/AKT/MTOR* signalling was involved in MEL-induced regulation towards autophagy.

To preliminarily confirm our assumption that *PI3K-AKT-MTOR* signalling is involved in MEL-induced regulation towards autophagy, further experiments were carried out. As shown in Figure 4b, the treatment of MEL increased the expression of LC3BII and inhibited the phosphorylation level of PIK3CA and AKT, which suggests that the autophagic level was enhanced and the activities of PIK3CA and AKT were decreased. Additionally, the basal phosphorylation level of TSC2 was reduced in MEL-treated aged BMMSCs (Figure 4b). The downregulated phosphorylation of MTOR was observed in MEL-treated aged BMMSCs, while the level of MTOR did not significantly change (Figure 4b), revealing that the decrease of MTOR activity might be involved in MEL-induced autophagy. These results support the hypothesis that the *PIK3CA-AKT-MTOR* pathway contributes to MEL-regulated autophagy.

To further investigate the mechanism of MEL-induced autophagy, BMMSCs were co-treated with MEL and the *PI3K-AKT-mTOR* pathway activator. Following co-treatment with MEL and the PI3KCA activator 740Y-P, the phosphorylation levels of AKT, PI3KCA, and mTOR increased compared to BMMSCs treated with MEL alone, which contrasted with the decreased phosphorylation level of TSC2 (Figure 4b). In conclusion, these results indicate that exposure to MEL (10 nM) results in inactivation of the *PIK3CA-AKT* signalling, then leads to upregulation of TSC2 activity and the subsequent downregulation of MTOR activity.

The following experiments were applied to further confirm whether the inhibition of MTOR signalling is necessary for MEL-regulated autophagy. RHEB<sup>Q64L</sup>, an active form that can activate *MTOR* signalling and stimulate the phosphorylation of MTOR, is transfected into aged BMMSCs to restore MTOR activity, as well as an inactive form of RHEB<sup>D60K</sup>. With RHEB<sup>Q64L</sup> overexpressing, the phosphorylation level of MTOR was upregulated in BMMSCs, suggesting that the activity of MTOR was restored with the transfection of RHEB<sup>Q64L</sup> (Figures 4c and 4d). Meanwhile, overexpression of RHEB<sup>Q64L</sup> eliminated the autophagy-inducing effects of MEL (Figures 4c and 4e). In contrast, overexpression of RHEB<sup>D60K</sup> failed to restore MTOR activity and the expression level of LC3BII (Figures 5c to 5e).

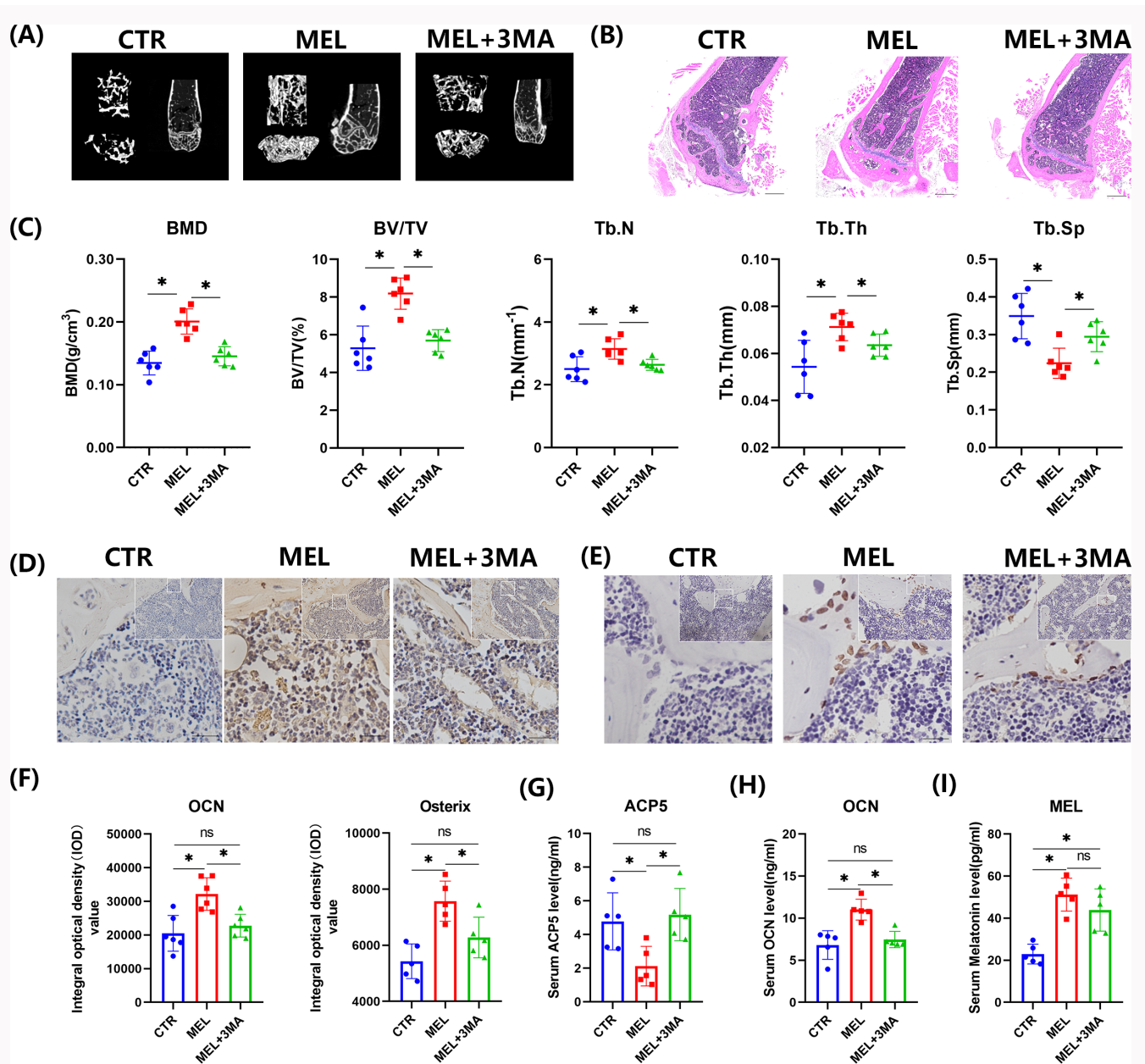


**Fig. 3**

Inhibition of autophagy could counteract melatonin (MEL)-induced osteogenic promotion in aged mice. a) Micro-CT ( $\mu$ CT) imaging of distal femora and b) haematoxylin and eosin (H&E) staining (40 $\times$ ) of proximal tibiae of aged mice treated with MEL for six weeks (50 mg kg<sup>-1</sup> body weight per day). c) Bone microstructure parameters such as bone mineral density (BMD), trabecular bone volume per total volume (BV/TV), trabecular bone thickness (Tb.Th), trabecular bone number (Tb.N), and trabecular bone separation (Tb.Sp) were measured by  $\mu$ CT scanning. d) to f) Immunohistopathology (200 $\times$ ) showed the osteogenic-related protein presentations of d) matricellular molecular osteocalcin (OCN) and e) osteogenic marker Osterix in proximal tibia bone tissue, and f) integral optical density (IOD) was calculated. g) to i) Concentrations of g) bone resorption marker ACP5, h) osteogenic marker OCN, and i) MEL in serum were analyzed by enzyme-linked immunosorbent assay (ELISA). \* $p < 0.05$ , significant differences between each indicated group analyzed using Fisher's exact test, one-way analysis of variance (ANOVA), or Tukey's post-hoc test. CTR, control group; ns, not significant.

These data reveal that the *PIK3CA-AKT-MTOR* signalling pathway is involved in MEL-induced autophagy.

#### MEL-GelMA system has therapeutic effects on bone fracture healing in aged mice

To enhance bone fracture healing through local administration of MEL, we incorporated MEL or MEL combined with 3MA into a GelMA material, which was then photocured at the fracture site following an open femoral mid-shaft fracture in aged mice. The compressive modulus, percentage mass remaining, and diffusional coefficient of the three material systems were

tested according to our previous research (Supplementary Figure d). After four weeks, radiographs,  $\mu$ CT (Figures 5a to 5c), and H&E staining (Figure 5d) showed an enhancement of bone fracture healing in MEL-treated mice and 3MA could counteract the MEL-induced osteogenesis promotion. Topical administration of MEL led to a higher union rate of fractured bone, while the controls showed arrest of fracture healing with only trace amounts of cartilaginous callus present (Figure 5b). The bone volume and BMD in the callus area in mice treated with MEL was greater by almost twofold relative to

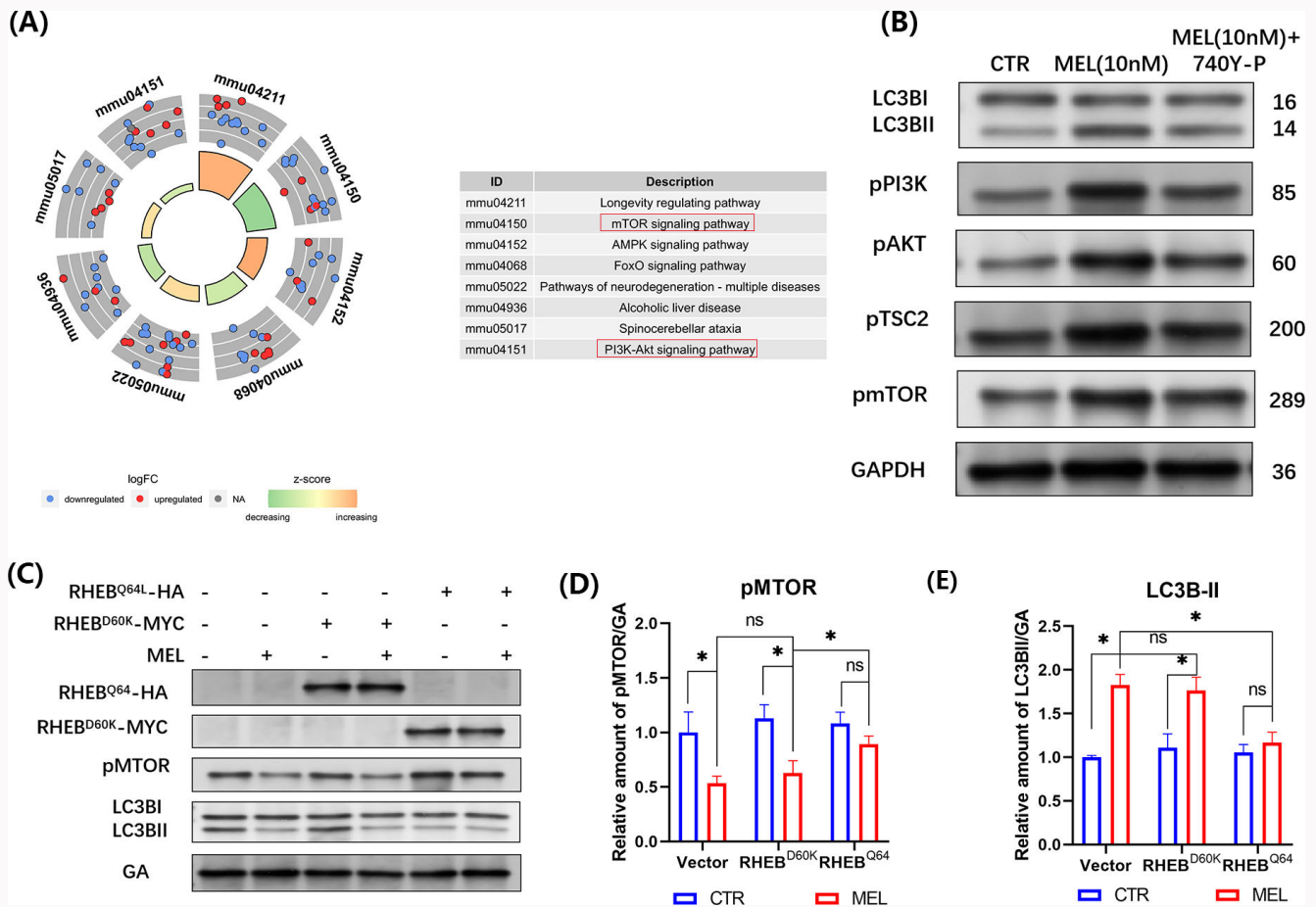


**Fig. 4**

PI3K-AKT-MTOR signalling is involved with melatonin (MEL) triggered autophagy in aged bone marrow-derived mesenchymal stem cells (BMMSCs). a) Top 10 Kyoto Encyclopedia of Genes and Genomes (KEGG) terms were analyzed, and the genes had a high enrichment in the MTOR pathway and PI3K-AKT pathway. b) Western blot analysis showed total and phosphorylation levels of microtubule-associated protein 1A/1B-light chain 3 beta (LC3B), PI3K-AKT, Tuberosus Sclerosis Complex 2 (TSC-2), and MTOR in cells treated with MEL or MEL + PI3K pathway activator 740-Y-P. c) to e) BMMSCs were first treated with MEL or PBS for 24 hrs, then transfected with vectors expressing constitutively active (Q64L) or inactive (D60K) ras homolog enriched in brain (RHEB) mutants for 24 hrs. c) BMMSC extracts were analyzed by western blotting. Protein levels of d) pMTOR and e) LC3B-II were detected as indicated. \* $p < 0.05$ , significant differences between each indicated group analyzed using one-way analysis of variance (ANOVA) or Tukey's post-hoc test. AMPK, adenosine 5'-monophosphate-activated protein kinase; CTR, control group; FoxO, Forkhead box O; GAPDH, glyceraldehyde-3-phosphate dehydrogenase; mTOR, mechanistic target of rapamycin; ns, not significant; PI3K-AKT, phosphatidylinositol 3 kinase-RAC- $\alpha$  serine/threonine-protein kinase.

controls, and 3MA could counteract MEL-induced osteogenesis promotion (Figure 5c).

To explore the underlying mechanisms of MEL's positive effects on bone fracture healing, H&E staining (Figure 5d) of the fractured femur demonstrated differences in tissue composition. The ratio of newly formed bone, cartilage, and fibrous tissue areas, along with the quantification of the new bone formation area, indicated enhanced healing in the MEL-treated group (Figures 5d and 5e). Specifically, the MEL group exhibited a greater area and proportion of newly formed bone compared to the GelMA and control groups. However, the application of 3MA partially counteracted this therapeutic effect, reducing the extent of new bone formation (Figures 5d and 5e). Immunohistopathology (Figure 5f) showed that the osteogenic-related protein OCN was more pronounced in the fracture callus of the MEL group, and IOD analysis confirmed these findings. Additionally, the number of osteoblasts (N.Ob/B.Pm) in the fracture callus was significantly higher in the MEL group compared to controls (Figure 5g), while the number of osteoclasts (N.OC/T.Ar) was notably lower,

as determined by TRAP staining (Figure 5h). To elucidate the relationship between autophagy and MEL-induced osteogenic effects, protein analysis from BMMSCs extracted after fracture healing (Figure 5i) revealed higher levels of the autophagy markers LC3BII and Beclin1, alongside elevated OCN levels, in the MEL group compared to the control and GelMA groups. In contrast, the addition of the autophagy inhibitor 3MA resulted in decreased LC3BII, Beclin1, and OCN levels, indicating that autophagy plays a crucial role in MEL's osteogenic regulatory effects. Taken together, these results provide evidence that MEL may have clinical utility in enhancing fracture healing and treating disorders of low bone mass such as senile osteoporosis.

## Discussion

With ageing, the declined ability of BMMSCs to differentiate into bone cells leads to osteoporosis.<sup>21</sup> Previous studies have suggested that three stages of osteogenic differentiation – osteogenic lineage commitment,<sup>22</sup> matrix synthesis,<sup>23</sup> and matrix mineralization<sup>24</sup> – showed degenerative changes

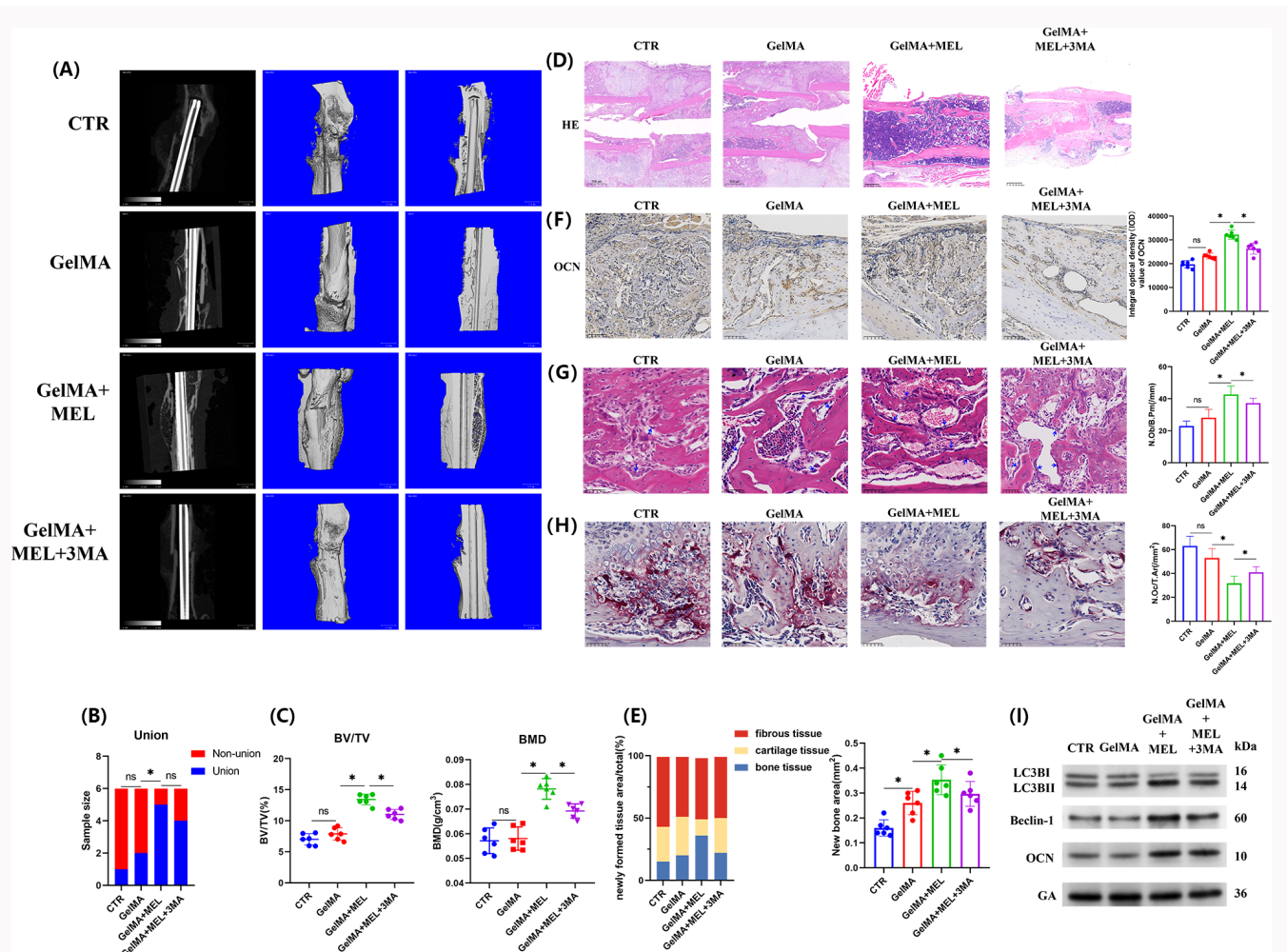


**Fig. 5**

Administration of melatonin (MEL) has therapeutic effects on bone fracture healing in aged mice. a) Representative radiograph and micro-CT ( $\mu$ CT) of femora in aged mice (n = 6 per group) four weeks after open femoral mid-shaft fracture. b) Nonunion frequency and c)  $\mu$ CT measurement of bone volume per total volume (BV/TV) and bone mineral density (BMD) in callus area of the fractured femora four weeks after open femoral mid-shaft fracture. d) Haematoxylin and eosin (H&E) staining (50 $\times$ ) of fractured femur. e) Ratio of newly formed bone, cartilage, and fibrous tissue area and quantification of the area of new bone formation. f) Immunohistochemistry (200 $\times$ ) of fractured femur, showing the osteogenic-related protein matricellular protein osteocalcin (OCN) in the fracture callus. The integral optical density (IOD) of OCN was calculated. g) Osteoblast counts in the fracture callus were assessed by counting the number of osteoblasts on each H&E-stained section, with osteoblast number/bone perimeter (N.Ob/B.Pm) (/mm) determined using Image-Pro Plus software (Media Cybernetics, USA). Blue arrows indicate typical osteoblasts in the sections, highlighting their distribution in the fracture callus. h) Evaluation of osteoclasts in fracture callus. The numbers of osteoclasts were counted based on tartrate-resistant acid phosphatase (TRAP)-stained sections, and osteoblast number/total area (N.OC/T.Ar) (/mm<sup>2</sup>) was determined by Image-Pro Plus software. i) Protein presentations from bone marrow-derived mesenchymal stem cells (BMMSCs) extracted from tibiae after fracture healing of autophagy markers LC3BI, Beclin, and the osteogenesis marker OCN. \*p < 0.05, significant differences between each indicated group analyzed using Fisher's exact test, one-way analysis of variance (ANOVA), or Tukey's post-hoc test. CTR, control group; GelMA, methacrylated gelatin; ns, not significant.

during the process of ageing. Our study has shown that mineralization ability was decreased, and the expression of osteogenic genes *runx2*, *osterix*, *col-1*, and *ocn* was significantly reduced compared with young BMMSCs, which confirmed that three stages of osteogenic differentiation all attenuated with ageing.

Age-related reduction in MEL in serum is considered to be a critical factor in bone loss and osteoporosis with ageing.<sup>25</sup> The MEL concentration in the human physiological environment is around 10<sup>-9</sup> M. We have proved in a previous study that MEL of close to physiological concentrations can promote the osteogenic differentiation of BMMSCs in a mouse model of oestrogen-deficient osteoporosis.<sup>12</sup> Consequently, a relatively lower dose of MEL (10 nM and 100 nM) was adopted in our study to imitate human physiological conditions. In

the present study, only MEL of 10 nM promoted osteogenic ability of BMMSCs from aged mice. Slower metabolism and proliferation in aged cells might contribute to lower tolerance to drug treatment,<sup>26</sup> so a relatively high concentration of MEL could decrease the proliferation in aged BMMSCs. Treatment with MEL (50 mg/kg body weight per day) exerted therapeutic effects in aged mice, as evidenced by increased BMD and improved bone structure. This may be attributed to the oral supplementation compensating for the reduced MEL levels in aged mice. However, although the increased risk of brain tumours and the possibility of behavioural changes were not observed in this study, these potential risks cannot be ignored.<sup>27,28</sup> Further research is therefore necessary to fully assess the adverse effects that may arise from long-term MEL use, ensuring its safety in clinical applications.

Despite the positive effects of MEL on bone, it does not influence the entire process of osteogenesis. In the present study, MEL enhanced the expression of *Runx2*, *osterix*, *ocn*, and *opg/rankl* ratio in aged BMMSCs. However, the expression of *col-1* remained unchanged with low doses of MEL in aged BMMSCs (Supplementary Figure be), which is inconsistent with a previous study showed an increase in *col-1* levels following MEL treatment.<sup>29</sup> Different concentration, varying microenvironments, and distinct cell origins might lead to the contradictory results. Our research indicates that MEL, at physiological concentrations, can promote early osteoblast differentiation, particularly during stages of cell commitment, mineralization, osteogenesis, and the balance between osteoblasts and osteoclasts. However, it does not appear to affect extracellular matrix maturation.

Autophagy is a degradation pathway triggered by complex transcription factors, and plays an important role in enormous physiological processes.<sup>30</sup> Increasing studies obtained accumulating evidence that MEL has functions of regulating and restoring autophagy in different physiological pathological changes.<sup>4</sup> We have found that MEL could increase autophagy in aged BMMSCs, and MEL exerted similar effects on autophagy in bone tissue in vivo, which may be attributed to the effects of oral MEL supplementation on serum MEL concentration. Bioinformatics analysis methods are very important for key pathways in osteoporosis.<sup>31</sup> We found that the MTOR pathway is related to MEL-induced autophagy through the KEGG enrichment method. A recent study indicated that MTOR pathways play an important role as an essential energy sensor, contributing to metabolic regulating and helping cells to adapt to unfavourable conditions.<sup>32</sup> In the present study, both the application of a PI3KCA activator and a constitutively active form of RHEB, which activates MTOR protein kinase activity, were able to negate the MEL-induced promotion of autophagy in aged BMMSCs. These results indicate that MEL regulates autophagy in aged BMMSCs via the PI3KCA-AKT-MTOR pathway.

Accumulating evidence has verified a role for autophagy in the occurrence and development of osteoporosis. A previous study has suggested that autophagy-related genes are related to occurrence and development of osteoporosis, according to human genome-wide association data.<sup>33</sup> Autophagy in osteoblasts is involved in mineralization and bone homeostasis. Inhibition of autophagosome formation in mice leads to severe osteopenia.<sup>5</sup> In different osteoporosis models, different changes in autophagy were observed. As reported, MEL suppressed autophagy in osteoblasts harvested from type 2 diabetic osteoporosis,<sup>34</sup> while another study indicated that decreased autophagy leads to degenerative changes of BMMSCs in mice with oestrogen deficiency-induced osteoporosis.<sup>35</sup> In line with our study, BMMSCs exhibited decreased autophagy levels in aged mice in a model of senile osteoporosis, and autophagy activator rapamycin could induce bone differentiation in aged BMMSCs and restore bone loss in aged mice.<sup>35</sup> In the present study, MEL can reverse bone loss and degenerative changes in elderly mice by increasing autophagy in vivo and in vitro, and the regulation of autophagy was involved in the promoting effects of MEL on osteogenesis. We speculate that a certain range of autophagy ability is essential for maintaining the osteogenic ability of BMMSCs. In different models, autophagy of a too

high<sup>34</sup> or too low<sup>35</sup> level could reduce osteogenic differentiation of BMMSCs. Thus, the reversal of the abnormal autophagic state has the potential to treat osteoporosis. It is clearly shown in our study that one of these important mechanisms involved in the positive role of MEL is autophagy. In addition, we have found in previous research that nuclear factor kappa B (*NF- $\kappa$ B*) signalling coupled the process of osteogenesis and osteoclastogenesis after MEL treatment.<sup>12</sup> Therefore, the beneficial effects of MEL might be coordinated by different signalling pathways.

Given the fact that bone fracture is the most serious clinical complication of osteoporosis, the potential of employing MEL as an alternative approach has attracted wide attention for improving bone healing. Bone regeneration is a well-orchestrated process with a specific time frame. It is considered advantageous that the bioactive substances are slowly and continuously released. Biomaterials can overcome the low tissue retention associated with MEL, and offer a controlled release platform for healing fractured bone.<sup>36</sup> GelMA provides sufficient space for drug loading, and drug release can be controlled through degradation.<sup>37,38</sup> In a recent study, GelMA loaded with highly ordered hollow micro-frustum-arrays using double-layer lithography facilitates the achievement of cellular osteodifferentiation, and enhances bone repair efficiency in a model of femoral fracture in vivo in mice.<sup>39</sup> MEL can influence osteogenesis both directly and indirectly. Directly, MEL promotes osteogenic differentiation by activating signalling pathways such as the *BMP/Smad* and *Wnt/ $\beta$ -catenin* pathways, which are crucial for bone formation.<sup>40</sup> Indirectly, MEL modulates the bone microenvironment by influencing the release of growth factors, cytokines, and other signalling molecules that support bone regeneration and repair as proven in the present study. The enhanced bone healing observed in the MEL-treated fractured femur, with a greater area and proportion of newly formed bone, confirms the osteogenic potential of MEL. The osteoblast counts in the MEL-treated fractured callus were significantly higher, while the osteoclast counts were reduced, indicating that MEL improved the osteoblast-osteoclast balance in aged mice with fracture. This improved osteoblast-osteoclast axis highlights MEL's positive regulatory effect on both bone formation and resorption.<sup>12</sup> However, the application of the autophagy inhibitor 3MA partially diminished these beneficial effects, reducing the new bone formation and osteoblast presence, further supporting the role of autophagy in MEL's osteogenic regulatory mechanisms. These combined effects contribute to its role in enhancing fracture healing and preventing bone loss in osteoporosis, albeit through distinct mechanisms. While bone morphogenetic protein 2 (BMP2) is widely recognized for its potent osteoinductive properties and is considered the gold standard,<sup>41</sup> MEL also shows promise as an autophagy regulator and osteogenic agent, with both direct and indirect effects on bone healing. However, it is important to note that MEL may not yet achieve the same level of effectiveness in promoting fracture healing as BMP2. MEL-loaded gel offers a potentially more cost-effective alternative, whereas BMP2 has a stronger track record in clinical settings.<sup>41</sup> Future studies should directly compare the efficacy of MEL-loaded gel with BMP-2 in a controlled setting to provide more definitive guidance for clinicians and a deeper understanding of MEL's potential role in clinical practice. Additionally, the synergistic

effects of BMP-2 and MEL in promoting fracture healing and treating osteoporosis need further exploration, as MEL has been shown to upregulate the gene expression of BMP-2, BMP-6, OCN, and Osterix, thereby enhancing osteogenesis through the activation of melatonin receptor 2 (MT<sub>2</sub>).<sup>25</sup> The MEL + GelMA system can encase the bone defect model non-invasively, thus avoiding contamination from invasive materials. Collectively, these results suggest that the MEL + GelMA system supports bone regeneration through the upregulation of autophagy.

In conclusion, according to our findings above, we summarize that MEL can alleviate degenerative osteogenesis of aged BMMSCs through regulating autophagy via the PIK3C-AKT-MTOR pathway, and that the MEL + GelMA system could help to promote bone fracture healing.

### Supplementary material

Figures showing the fracture healing promoting and age-related osteoporosis alleviating effects of melatonin (MEL), a representative image of part of fracture callus of a healing murine fractured femur, degenerative properties of aged bone marrow-derived mesenchymal stem cells (BMMSCs) in osteogenesis, the diverse effects of different concentrations of MEL on osteogenesis of BMMSCs in vitro, and the material properties of methacrylated gelatin (GelMA), GelMA + MEL (10mM), and GelMA + MEL (10mM) + 3MA (5mM) system. Table showing quantitative real-time reverse transcriptase polymerase chain reaction (RT-PCR) primers. An ARRIVE checklist is also included to show that the ARRIVE guidelines were adhered to in this study.

### References

- Chin KY, Ima-Nirwana S. The role of tocotrienol in preventing male osteoporosis—a review of current evidence. *Int J Mol Sci.* 2019;20(6):1355.
- Nuti R, Brandi ML, Checchia G, et al. Guidelines for the management of osteoporosis and fragility fractures. *Intern Emerg Med.* 2019;14(1):85–102.
- Qadir A, Liang S, Wu Z, Chen Z, Hu L, Qian A. Senile osteoporosis: the involvement of differentiation and senescence of bone marrow stromal cells. *Int J Mol Sci.* 2020;21(1):349.
- Boga JA, Caballero B, Potes Y, et al. Therapeutic potential of melatonin related to its role as an autophagy regulator: a review. *J Pineal Res.* 2019;66(1):e12534.
- Nollet M, Santucci-Darmanin S, Breuil V, et al. Autophagy in osteoblasts is involved in mineralization and bone homeostasis. *Autophagy.* 2014;10(11):1965–1977.
- Talib WH. Melatonin and cancer hallmarks. *Molecules.* 2018;23(3):518.
- Wang X, Jiang W, Pan K, Tao L, Zhu Y. Melatonin induces RAW264.7 cell apoptosis via the BMAL1/ROS/MAPK-p38 pathway to improve postmenopausal osteoporosis. *Bone Joint Res.* 2023;12(11):677–690.
- Han Y, Kim YM, Kim HS, Lee KY. Melatonin promotes osteoblast differentiation by regulating Osterix protein stability and expression. *Sci Rep.* 2017;7(1):5716.
- Hill SM, Cheng C, Yuan L, et al. Age-related decline in melatonin and its MT<sub>1</sub> receptor are associated with decreased sensitivity to melatonin and enhanced mammary tumor growth. *Curr Aging Sci.* 2013;6(1):125–133.
- Carbone L. Pain management standards in the eighth edition of the Guide for the Care and Use of Laboratory Animals. *J Am Assoc Lab Anim Sci.* 2012;51(3):322–328.
- Doube M, Kłowski MM, Arganda-Carreras I, et al. BoneJ: free and extensible bone image analysis in ImageJ. *Bone.* 2010;47(6):1076–1079.
- Zhou Y, Wang C, Si J, et al. Melatonin up-regulates bone marrow mesenchymal stem cells osteogenic action but suppresses their mediated osteoclastogenesis via MT<sub>2</sub> -inactivated NF-κB pathway. *Br J Pharmacol.* 2020;177(9):2106–2122.
- Dempster DW, Compston JE, Drezner MK, et al. Standardized nomenclature, symbols, and units for bone histomorphometry: a 2012 update of the report of the ASBMR Histomorphometry Nomenclature Committee. *J Bone Miner Res.* 2013;28(1):2–17.
- Zhang L, Chang M, Beck CA, Schwarz EM, Boyce BF. Analysis of new bone, cartilage, and fibrosis tissue in healing murine allografts using whole slide imaging and a new automated histomorphometric algorithm. *Bone Res.* 2016;4:15037.
- Alexander SPH, Roberts RE, Broughton BRS, et al. Goals and practicalities of immunoblotting and immunohistochemistry: a guide for submission to the British Journal of Pharmacology. *Br J Pharmacol.* 2018;175(3):407–411.
- Xu R, Yallowitz A, Qin A, et al. Targeting skeletal endothelium to ameliorate bone loss. *Nat Med.* 2018;24(6):823–833.
- Yu M, Ma L, Yuan Y, et al. Cranial suture regeneration mitigates skull and neurocognitive defects in craniosynostosis. *Cell.* 2021;184(1):243–256.
- No authors listed. GeneCards®: The Human Gene Database. Weizmann Institute of Science. <https://www.genecards.org/> (date last accessed 23 January 2025).
- No authors listed. DISGENET. MedBioinformatics Solutions SL. 2024. <https://disgenet.com/> (date last accessed 23 January 2025).
- No authors listed. OMIM®: An Online Catalog of Human Genes and Genetic Disorders. Johns Hopkins University. [www.omim.org](http://www.omim.org) (date last accessed 23 January 2025).
- Wang L, Niu N, Li L, Shao R, Ouyang H, Zou W. H3K36 trimethylation mediated by SETD2 regulates the fate of bone marrow mesenchymal stem cells. *PLoS Biol.* 2018;16(11):e2006522.
- Lin CH, Li NT, Cheng HS, Yen ML. Oxidative stress induces imbalance of adipogenic/osteoblastic lineage commitment in mesenchymal stem cells through decreasing SIRT1 functions. *J Cell Mol Med.* 2018;22(2):786–796.
- Du T, Liu N, Gu B, et al. Effects of aging on the proliferation and differentiation capacity of human periodontal ligament stem cells. *Chin Med Sci J.* 2017;32(2):83–1.
- Boskey AL, Coleman R. Aging and bone. *J Dent Res.* 2010;89(12):1333–1348.
- Li T, Jiang S, Lu C, et al. Melatonin: another avenue for treating osteoporosis? *J Pineal Res.* 2019;66(2):e12548.
- Palmer AK, Xu M, Zhu Y, et al. Targeting senescent cells alleviates obesity-induced metabolic dysfunction. *Aging Cell.* 2019;18(3):e12950.
- Kinker GS, Ostrowski LH, Ribeiro PAC, et al. MT<sub>1</sub> and MT<sub>2</sub> melatonin receptors play opposite roles in brain cancer progression. *J Mol Med (Berl).* 2021;99(2):289–301.
- Alghamdi BS. The effect of melatonin and exercise on social isolation-related behavioral changes in aged rats. *Front Aging Neurosci.* 2022;14:828965.
- Xu L, Zhang L, Wang Z, et al. Melatonin suppresses estrogen deficiency-induced osteoporosis and promotes osteoblastogenesis by inactivating the NLRP3 inflammasome. *Calcif Tissue Int.* 2018;103(4):400–410.
- Levine B, Kroemer G. Biological functions of autophagy genes: a disease perspective. *Cell.* 2019;176(1–2):11–42.
- Yuan W, Yang M, Zhu Y. Development and validation of a gene signature predicting the risk of postmenopausal osteoporosis. *Bone Joint Res.* 2022;11(8):548–560.
- Mihaylova MM, Shaw RJ. The AMPK signalling pathway coordinates cell growth, autophagy and metabolism. *Nat Cell Biol.* 2011;13(9):1016–1023.
- Pierrefite-Carle V, Santucci-Darmanin S, Breuil V, Camuzard O, Carle GF. Autophagy in bone: self-eating to stay in balance. *Ageing Res Rev.* 2015;24(Pt B):206–217.
- Zhang W-L, Meng H-Z, Yang R-F, et al. Melatonin suppresses autophagy in type 2 diabetic osteoporosis. *Oncotarget.* 2016;7(32):52179–52194.
- Qi M, Zhang L, Ma Y, et al. Autophagy maintains the function of bone marrow mesenchymal stem cells to prevent estrogen deficiency-induced osteoporosis. *Theranostics.* 2017;7(18):4498–4516.
- Nižić L, Potaš J, Winnicka K, et al. Development, characterisation and nasal deposition of melatonin-loaded pectin/hypromellose microspheres. *Eur J Pharm Sci.* 2020;141:105115.
- Pacelli S, Rampetsreiter K, Modaresi S, et al. Fabrication of a double-cross-linked interpenetrating polymeric network (IPN) hydrogel surface

modified with polydopamine to modulate the osteogenic differentiation of adipose-derived stem cells. *ACS Appl Mater Interfaces*. 2018;10(30):24955–24962.

38. **Jalili NA, Jaiswal MK, Peak CW, Cross LM, Gaharwar AK.** Injectable nanoengineered stimuli-responsive hydrogels for on-demand and localized therapeutic delivery. *Nanoscale*. 2017;9(40):15379–15389.
39. **He J, You D, Li Q, et al.** Osteogenesis-inducing chemical cues enhance the mechanosensitivity of human mesenchymal stem cells for

osteogenic differentiation on a microtopographically patterned surface. *Adv Sci (Weinh)*. 2022;9(16):e2200053.

40. **Malakoti F, Zare F, Zarezadeh R, et al.** The role of melatonin in bone regeneration: a review of involved signaling pathways. *Biochimie*. 2022;202:56–70.
41. **Tsuji K, Bandyopadhyay A, Harfe BD, et al.** BMP2 activity, although dispensable for bone formation, is required for the initiation of fracture healing. *Nat Genet*. 2006;38(12):1424–1429.

### Author information

**D. Zhang**, PhD, Research Fellow  
**T. Zhu**, PhD, Research Fellow  
**J. Bai**, PhD, Research Fellow  
**C. Chen**, MD, Research Fellow  
**J. Wen**, PhD, Senior Lecturer  
**Y. Zhou**, PhD, Professor  
**X. Guan**, PhD, Senior Lecturer  
The Affiliated Hospital of Stomatology, School of Stomatology, Zhejiang University of Medicine, and Key Laboratory of Oral Biomedical Research of Zhejiang Province, Hangzhou, China.

### Author contributions

D. Zhang: Conceptualization, Data curation, Formal analysis, Investigation, Writing – original draft.  
T. Zhu: Conceptualization, Investigation, Writing – original draft.  
J. Bai: Investigation.  
C. Chen: Visualization.  
J. Wen: Investigation.  
Y. Zhou: Project administration, Supervision, Writing – review & editing.  
X. Guan: Project administration, Supervision, Writing – review & editing.

### Funding statement

The author(s) disclose receipt of the following financial or material support for the research, authorship, and/or publication of this article: this research was supported by Zhejiang Provincial Natural Science Foundation of China under Grant No. LY23H140001, the Key International (Regional) Cooperative Research, Project of the National Nature Science Foundation of China, grant number 82020108011, and National Natural Science Foundation of China (Grant Number: 82071085), as reported by X. Guan and Y. Zhou. The funding body played no role in the design of the study and collection, analysis, and interpretation of data and in writing the manuscript.

### ICMJE COI statement

X. Guan reports a grant from Zhejiang Provincial Natural Science Foundation of China under Grant No. LY23H140001, related to this study. Y. Zhou reports grants from: the Key International (Regional) Cooperative Research, Project of the National Nature Science Foundation of China, grant number 82020108011; and the National Natural Science Foundation of China (Grant Number: 82071085), both related to this study.

### Data sharing

The data that support the findings for this study are available to other researchers from the corresponding author upon reasonable request.

### Acknowledgements

The authors thank Dr Chaowei Wang from Zhejiang University for her technical guidance in the experiments.

### Ethical review statement

All animal experiments were approved by the Animal Ethics Committee of Zhejiang University (No. ZJU20220168).

### Open access funding

The authors report that the open access funding for their manuscript was self-funded.

© 2025 Zhang et al. This is an open-access article distributed under the terms of the Creative Commons Attribution Non-Commercial No Derivatives (CC BY-NC-ND 4.0) licence, which permits the copying and redistribution of the work only, and provided the original author and source are credited. See <https://creativecommons.org/licenses/by-nc-nd/4.0/>